All-Epitaxial $Fe_{5-x}GeTe_2/Graphene$ and $Fe_{5-x}GeTe_2/WSe_2$ van der Waals Heterostructures With Above Room Temperature Ferromagnetism

Hua Lv¹, Jens Herfort¹, Michael Hanke¹, Chen Chen², Joan M. Redwing¹⁰², Achim Trampert¹⁰¹, Roman Engel-Herbert¹, Manfred Ramsteiner¹⁰¹, and Joao Marcelo J. Lopes¹⁰¹

¹Paul-Drude-Institut für Festkörperelektronik, Leibniz-Institut im Forschungsverbund Berlin e.V, 10117 Berlin, Germany
²2D Crystal Consortium Materials Innovation Platform, Materials Research Institute, The Pennsylvania State University, University Park, PA 16802 USA

Van der Waals (vdW) heterostructures combining 2-D ferromagnets and other nonmagnetic layered materials, such as graphene and WSe₂, are highly promising for the realization of novel spintronic devices with integrated magnetic, electronic, and optical functionalities. Among different 2-D ferromagnets, $Fe_{5-x}GeTe_2$ ($x \sim 0$) shows a high potential due to its high Curie temperature (T_C). Furthermore, compared to commonly used top-down flake stacking strategies, large-scale, all-epitaxial vdW heterostructures are compatible with modern technologies and thus crucial for practical applications. In this contribution, we report on scalable epitaxial growth of $Fe_{5-x}GeTe_2$ via molecular beam epitaxy (MBE) on single-crystalline graphene (on SiC) and WSe₂ (on Al₂O₃) templates. Structural characterizations show the good crystalline quality of the epitaxial $Fe_{5-x}GeTe_2$ films on graphene and WSe₂. Importantly, magnetotransport investigations indicate a ferromagnetic order above room temperature for both $Fe_{5-x}GeTe_2$ /graphene with perpendicular magnetic anisotropy (PMA) and $Fe_{5-x}GeTe_2$ /WSe₂ (with low-temperature PMA) heterostructures. Moreover, an unconventional Hall effect (UHE) has been observed in both $Fe_{5-x}GeTe_2$ /graphene and $Fe_{5-x}GeTe_2$ /WSe₂ heterostructures, indicating the formation of topological spin structures. These results represent an important advance regarding bottom-up synthesis of vdW heterostructures beyond conventional exfoliation-based methods, which is crucial for the development of future spintronic applications based on 2-D magnetic materials.

Index Terms—2-D magnetic materials, 2-D spintronics, epitaxial films, van der waals (vdW) magnets.

I. INTRODUCTION

TWO-DIMENSIONAL magnetic materials show great promise for realizing novel and ultracompact spintronic devices [1]. Furthermore, building van der Waals (vdW) heterostructures by combining 2-D magnets and other non-magnetic materials, such as graphene and semiconducting transition metal dichalcogenides (e.g., WSe₂), is a very attractive pathway to integrate different functionalities of each 2-D material, as well as to enable new ones via proximity-induced phenomena taking place at the vdW heterointerfaces [2]. Importantly, vdW heterostructures with atomically sharp interfaces are expected to overcome long-term challenges faced by conventional heterostructures built on 3-D materials, namely, strong interface intermixing and large interface roughness, which can result in magnetic dead layers [3].

The state-of-the-art magnetic vdW heterostructures are mostly fabricated by using a top-down strategy through sequential stacking of flakes exfoliated from bulk crystals [4]. However, the exfoliation-based methods are not scalable and difficult to integrate into the standard device fabrication processes, which require high-quality materials deposited on a wafer scale. Therefore, developing bottom-up synthesis

Manuscript received 22 March 2024; revised 11 June 2024; accepted 8 July 2024. Date of publication 11 July 2024; date of current version 27 August 2024. Corresponding authors: H. Lv and J. M. J. Lopes (e-mail: hua.lv@pdi-berlin.de; lopes@pdi-berlin.de).

Color versions of one or more figures in this article are available at https://doi.org/10.1109/TMAG.2024.3426954.

Digital Object Identifier 10.1109/TMAG.2024.3426954

methods, such as thin-film epitaxial growth, is crucial to realize uniform 2-D magnetic films and heterostructures with high structural quality for integration in the next-generation spintronic technologies [3]. In this respect, molecular beam epitaxy (MBE) growth is one of the methods showing a great prospect owing to its fine control of individual elements during synthesis process. In fact, progress has recently been made in terms of MBE growth of 2-D magnetic materials and related heterostructures [5], [6], [7], [8].

From an application perspective, it is critical that the adopted 2-D magnets should sustain magnetic order above room temperature (RT). Recently, the 2-D Fe–Ge–Te compounds have been found to be promising candidates among other 2-D ferromagnets due to their relatively high Curie temperatures ($T_{\rm C}$) [9], [10]. They possess a layered structure with each single layer being formed of Fe and Ge slabs encapsulated by the layers of Te [1]. While $T_{\rm C} \approx 220~{\rm K}$ and 270 K have been reported for Fe₃GeTe₂ [5] and Fe₄GeTe₂ [11], respectively, the Fe_{5-x}GeTe₂ phase (FGT, with $x \approx 0$) can sustain ferromagnetism up to or even above 300 K [10], [12], which makes this material very promising for the development of novel 2-D spintronic devices.

In this work, we report on the realization of large-area epitaxial growth of FGT thin films via MBE directly on 2-D nonmagnetic graphene and WSe₂ templates, both also synthesized by an epitaxial method. Structural characterization confirms that homogeneous epitaxial vdW heterostructures exhibiting good structural quality can be realized. Moreover,

0018-9464 © 2024 IEEE. Personal use is permitted, but republication/redistribution requires IEEE permission. See https://www.ieee.org/publications/rights/index.html for more information.

magnetotransport investigations reveal promising magnetic properties for the FGT/graphene and FGT/WSe₂ material systems, including room-temperature ferromagnetism. They are comparable or even superior to what has been reported for similar systems prepared with flakes exfoliated from bulk single crystals.

II. EXPERIMENT

A. Sample Growth and Structural Characterization

FGT films were grown by MBE using elemental fluxes of Fe, Ge, and Te evaporated from Knudsen cells. For the flux ratios utilized in this study, Rutherford backscattering spectrometry revealed an average composition of Fe_{4.8}GeTe₂ [12]. Thin films with thicknesses ranging from 10 to 17 nm (corresponding to 10–17 FGT single layers; 1 single layer is ≈ 1 nm thick [10]) were grown at a substrate temperature of 300 °C on single crystalline, continuous monolayer-bilayer thick graphene [on SiC(0001)] and WSe₂ [on Al₂O₃(0001)]. These templates are also epitaxially grown on their substrates via SiC surface graphitization [13] and chemical vapor deposition (CVD) [14], respectively. Before FGT growth, both substrates were outgassed in situ at the 300 °C-450 °C temperature range in order to remove surface contaminants. After FGT growth, a 5 nm thick Te capping was deposited at RT aiming at the protection of the FGT surface against oxidation upon air exposure. The structural characterization of the samples with different methods, such as X-ray diffraction (XRD), atomic force microscopy (AFM), and scanning transmission electron microscopy (STEM), confirmed the epitaxial nature of the FGT films on graphene and WSe2, their layered crystalline structure, as well as the generally sharp nature of the vdW interfaces.

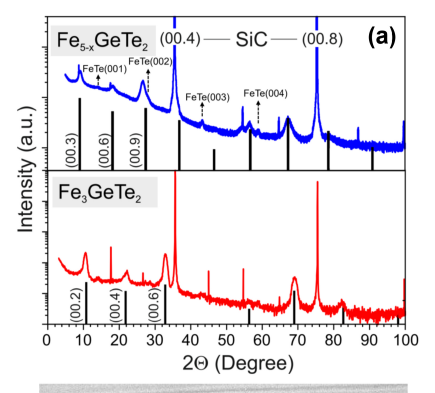
B. Magnetotransport Characterization

Magnetotransport measurements were performed at temperatures ranging from 4.3 to 400 K with an external perpendicular (z-direction) magnetic field of up to 0.8 T under vacuum conditions (10^{-6} – 10^{-5} mbar). The samples were bonded on a chip carrier with Al contact wires. For FGT/graphene samples, rectangular stripes of the sample were used. A constant current was applied along the long side (x-direction) through two contacts close to the edges of the strip. To determine the longitudinal resistance, the voltage (V_{xx}) was measured between two inner contacts. The Hall voltage (V_{xy}) was measured in the orthogonal direction (y-direction) between two contacts close to the center of the strip [12]. For FGT/WSe₂ samples, the measurements were carried on Hall bar structures fabricated by standard photolithography.

III. RESULTS AND DISCUSSION

A. Structural Properties

Fig. 1(a) (top) depicts a typical out-of-plane omega-2theta XRD scan for a 10 nm thick FGT film grown on graphene/SiC(0001). The existence of a set of subsequent (00.n) reflections (n = 3, 6, 9, ...), which fits well to the



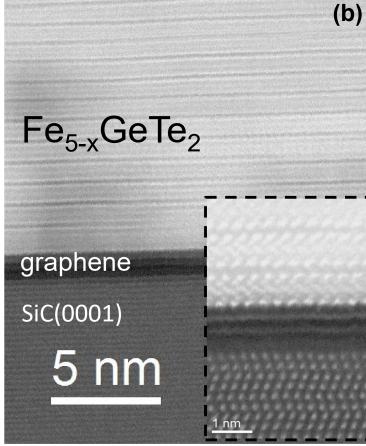


Fig. 1. Results for the structural characterization of the FGT films on graphene/SiC(0001). (a) (top) XRD scan for a 10 nm thick FGT film on graphene/SiC(0001) and FGT powder pattern bars; the reflections associated with tetragonal FeTe are also indicated; (bottom) XRD scan for 10 nm thick Fe₃GeTe₂ film on graphene/SiC(0001) plotted for comparison and the corresponding Fe₃GeTe₂ powder pattern bars. (b) (HAADF)-STEM image taken along the SiC [1–100] zone axis for a 15 nm thick FGT film on graphene/SiC(0001). The inset shows another image taken along the SiC [11–20] zone axis, where the interfacial region between the FGT film and bilayer graphene can be better visualized.

numerically derived powder pattern (black bars), confirms that the film exhibits the expected Fe₅GeTe₂ structure [10], [12]. The concurrent formation of the lower T_C Fe₃GeTe₂ phase can be ruled out. This can be concluded by comparing the results to an XRD scan obtained for an MBE-grown Fe₃GeTe₂ film as well as Fe₃GeTe₂ powder pattern bars, both also plotted in Fig. 1(a) (bottom). Finally, note that additional reflections can be identified in the FGT diffractogram, which shows an unintentional formation of the tetragonal FeTe phase (an anti-ferromagnet with a Néel temperature around 70 K) [15]. Further refinement of growth protocols is needed in order to mitigate the formation of this secondary phase. Finally, Fig. 1(b) shows high-angle annular dark-field (HAADF)-STEM images of the FGT/graphene heterostructure, where it is possible to observe the continuous, layered nature of the FGT film, and the sharp nature of its interface to the underlying graphene. In addition, the formation of FGT single layers with a thickness larger than that of Fe₅GeTe₂ can be observed (e.g., first FGT layer interfacing graphene). More specific discussion on this aspect can be found in [12]. The structural characterization of the FGT/WSe₂ films (not shown) revealed similarly good structural properties for the samples

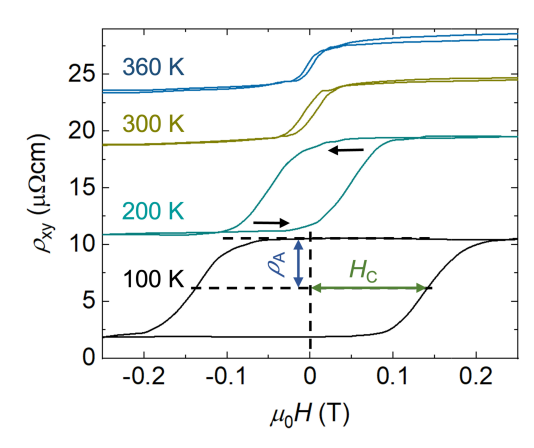


Fig. 2. AHE measured at different temperatures for a 10 nm thick FGT on graphene/SiC(0001), where a linear background caused by the OHE has been removed. The curves for temperatures above 100 K are successively upshifted for clarity. The definition of the quantities $\rho_{\rm A}$ and $H_{\rm C}$ is indicated by the blue and green double arrows, respectively. The black arrows indicate the sweeping direction of the perpendicular magnetic field.

and the epitaxial alignment between the 2-D layers. Detailed structural data on this system will be reported in the future.

B. Magnetic and Transport Properties of FGT/Graphene

We measured the anomalous Hall effect (AHE) to study the magnetic properties of the samples. Fig. 2 displays the AHE curves measured at different temperatures for a 10 nm thick FGT film on graphene/SiC(0001), where a linear background caused by ordinary Hall effect (OHE) has been removed. The black arrows indicate the sweeping direction of the perpendicular magnetic field. Since the Hall resistivity (ρ_{xy}) is proportional to the magnetization, the hysteresis curves of AHE are associated with the switching of the magnetization. Hysteresis loops measured up to 360 K show a clear coercivity, indicating a preferential perpendicular magnetic anisotropy (PMA) persisting above RT for the FGT/graphene heterostructures. In fact, the determination of $T_{\rm C}$ revealed a value around 390 K [12], which is higher than what has been reported in FGT flakes of comparable thicknesses exfoliated from bulk crystals [10]. Note that investigations via SQUID magnetometry corroborate the magnetotransport data [12]. The larger $T_{\rm C}$ as well as PMA of FGT films grown on graphene, in comparison to that of bulk crystals, might be associated with the presence of isolated single layers with Fe concentration higher than 5 [12]. Nevertheless, future investigations are required in order to address this aspect in detail. PMA above RT plays an important role in modern spintronics, such as low power consumption magnetic memories [3]. However, it is difficult to achieve a robust PMA in films of conventional 3-D ferromagnets unless their thickness is reduced to only a few nanometers [16]. The demonstrated PMA in our heterostructures containing relatively thick FGT films (10–15 nm) indicates their high potential for future spintronic applications [3].

Fig. 3(a) depicts the dependence of the anomalous Hall resistivity ρ_A (at magnetization saturation) on temperature for two FGT/graphene heterostructures with FGT thicknesses of 10 and 15 nm. Both samples exhibit a comparable trend, indicating a high reproducibility of the epitaxially grown

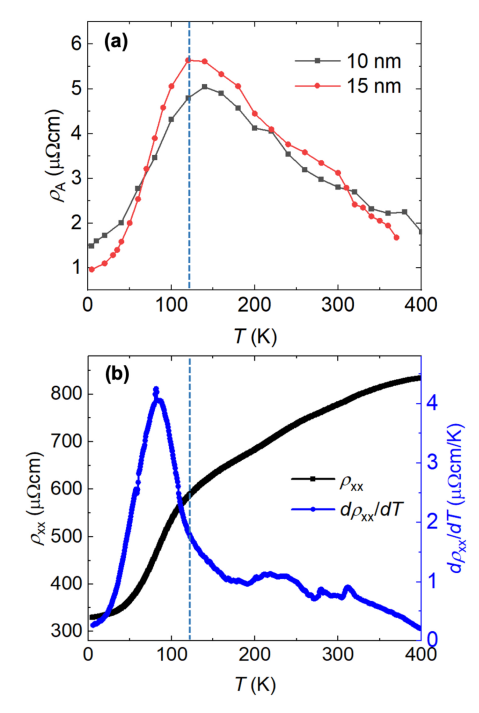


Fig. 3. (a) AHE resistivity $\rho_{\rm A}$ plotted as a function of temperature for 10 and 15 nm thick FGT films on graphene/SiC(0001). (b) Temperature-dependent longitudinal resistivity [ρ_{xx} , in black)] and its derivative ($d\rho_{xx}/dT$, in blue) for the 15 nm thick FGT/graphene sample. The cyan lines in (a) and (b) indicate the temperature of 120 K, around which a transition in both transverse and longitudinal transport is observed.

heterostructures. At about 120 K, a clear change of the temperature-dependent ρ_A is observed, which will be discussed in more detail later. Above 120 K, the monotonically reducing ρ_A suggests a smooth decrease in magnetization, without apparent further magnetic phase transitions [12]. Fig. 3(b) shows the temperature-dependent longitudinal resistivity (ρ_{xx}) and its derivative $(d\rho_{xx}/dT)$ for the 15 nm thick FGT/graphene system at H = 0. Overall, the temperaturedependent ρ_{xx} exhibits a metallic behavior with a clear change of its slope at around 120 K, consistent with previous reports on FGT flakes and bulk crystals [17], [18]. However, the plateau of $d\rho_{xx}/dT$ starting at 150 K remains up to a much higher temperature (well above 300 K) in comparison with previously reported results [11], [18], [19], which is consistent with the higher $T_{\rm C}$. Usually, the residual-resistance ratio (RRR), calculated as $\rho_{xx}(300 \text{ K})/\rho_{xx}(4.3 \text{ K})$, can be considered as an index of the degree of disorder of the material (the higher the RRR, the lower the degree of disorder) [17]. The RRR of 2.4 obtained is comparable or even higher than what has been reported for nanometer-thick flakes exfoliated from bulk single crystals [18], [19], indicating a comparable or lower degree of disorder. This is corroborated by the ρ_{xx} behavior at low temperature, which in the present case does not show a resistance upturn due to electron-electron interactions (EEI) promoted by disorder [17].

Finally, we discuss the possible origins of the transition at about 120 K observed in both transverse [Fig. 3(a)] and longitudinal transports [Fig. 3(b)]. It has been reported that FGT undergoes a permanent magnetostructural phase transition from a metastable precooling phase to a stable

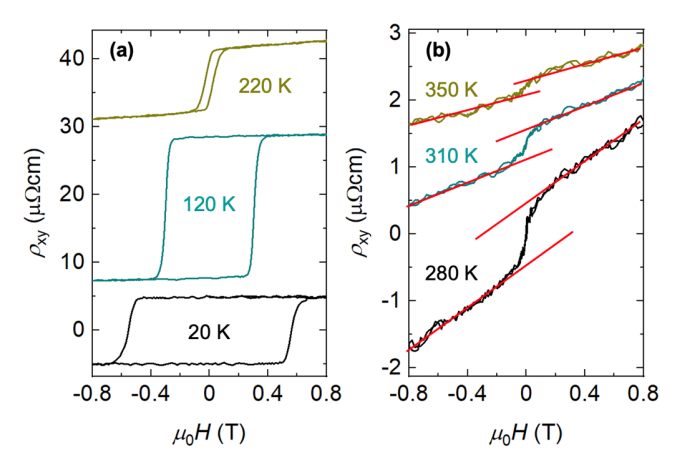


Fig. 4. AHE measured for a 17 nm thick FGT/WSe $_2$ heterostructure for (a) 20–220 K and (b) 280–350 K temperature ranges. The curves for temperatures above 20 K in (a) and 280 K in (b) are successively upshifted for clarity.

postcooling phase at about 100 K [20], [21]. However, this cannot explain the transition shown in Fig. 3(a) and (b) since our measurements were performed starting from a low temperature of 4.3 K. In FGT, different equivalent Fe atoms contribute differently to its magnetic and transport properties. Particularly, the moment of the Fe(1) sublattice, which is the closest to the vdW gap, is well ordered below 100 K but fluctuates significantly above 100 K [20], [22], [23]. This fluctuation dominates the carrier scattering in FGT. While below 120 K the ordered Fe(1) reduces the chance of spin-dependent carrier scattering, thus resulting in a decreased resistance, the enhancement of fluctuation of its moment with increasing temperature above 120 K leads to a decrease of magnetization and ρ_A [20].

C. Magnetic and Transport Properties of FGT/WSe2

The epitaxially grown FGT/WSe₂ heterostructures also exhibit ferromagnetism persisting at high temperatures, however with a temperature dependence that is different than the one observed for FGT/graphene. Fig. 4 displays the AHE curves measured in a 17 nm thick FGT/WSe₂ heterostructure fabricated to a Hall bar structure with a width of 40 μ m. The dependence of ρ_A on temperature exhibits the same transition at about 120 K, similar to that observed for the FGT/graphene system [Fig. 3(a)]. At low temperatures, the AHE loops exhibit a nearly squared shape with clear coercivity [Fig. 4(a)], indicating the occurrence of PMA. However, at high temperatures above 250 K, the loops display zero coercivity but exhibit a clear S shape at low field. Since ρ_{xy} exhibits a linear dependence at high field [see red lines in Fig. 4(b)], a typical two-carrier model cannot explain the S-shaped curves in this case, as in that case the two-carrier dominated Hall effect should exhibit a smooth round shape. Therefore, the linear behavior of ρ_{xy} at high field should be attributed to the OHE in FGT. The S-shaped ρ_{xy} at low field could be associated with a transition to a paramagnetic phase or to an in-plane magnetic anisotropy. This is in clear contrast to what is observed for the FGT/graphene samples, which exhibited a preferential PMA with finite coercivity throughout the entire measured temperatures from 4.3 K up to 360 K. Another interesting aspect

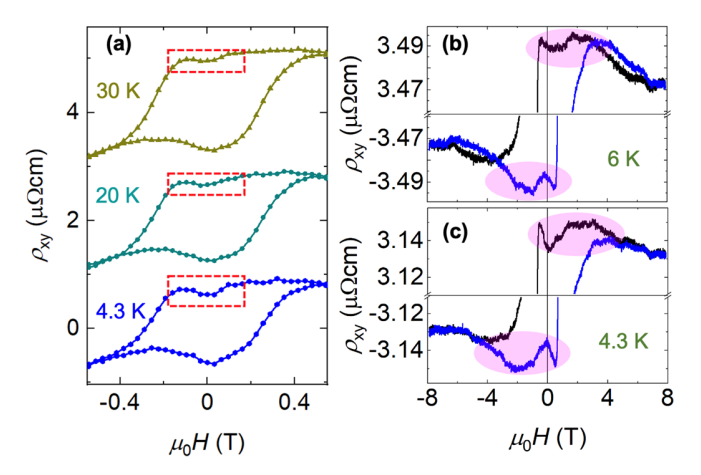


Fig. 5. UHE measured for (a) 15 nm FGT/graphene and (b) and (c) 17 nm FGT/WSe₂ epitaxial vdW heterostructures. The curves in (a) above 4.3 K are successively upshifted for clarity, while in (b) and (c), they are expanded around the magnetization switching for better visualization of the UHE.

is that the 17 nm FGT/WSe₂ heterostructures exhibit a larger $H_{\rm C}$ at low temperatures (e.g., 0.56 T at 20 K) with respect to that of the 10 and 15 nm FGT/graphene systems (e.g., ~ 0.3 T at 20 K). These differences in magnetic properties (e.g., magnetic anisotropy, $H_{\rm C}$) cannot be explained by a thickness-dependent behavior of FGT, given the comparable FGT thicknesses employed in both cases. It could be caused by structural differences in the FGT film grown in the different templates or by distinct coupling mechanisms taking place at the FGT/graphene and FGT/WSe2 interfaces, which are expected to influence the magnetic properties [8], [24], [25], [26]. Although more studies (e.g., structural investigations, thickness dependence) are required for obtaining an in-depth understanding of both systems, these results serve to underline the potential of vdW heterostructures for enabling property tailoring via heterostructure design.

D. Unconventional Hall Effect

The state-of-the-art FGT crystals have been shown to host topological spin structures, such as magnetic skyrmions [21]. More recently, noncoplanar magnetic structures resulted in an unconventional Hall effect (UHE) measured at low temperatures for FGT flakes [19]. Similar findings have been obtained for magnetotransport experiments conducted in Fe₃GeTe₂/WTe₂ vdW heterostructures built by sequential flake stacking [26]. In the latter case, the UHE (called by the authors topological Hall effect) was associated with a Dzyaloshinskii-Moriya interaction (DMI) induced at the Fe₃GeTe₂/WTe₂ vdW heterointerface. For the epitaxial FGT/graphene and FGT/WSe₂ heterostructures studied here, an UHE has also been observed at low temperatures, which we speculate to be associated with the formation of spin textures, possibly skyrmions [26], [27]. Fig. 5(a) depicts the results for the 15 nm thick FGT/graphene heterostructure. Differently from the usual square-shape AHE, the ρ_{xy} curves measured from 4.3 to up to 30 K exhibit an unusual shape that can be clearly identified during the magnetization switching, as highlighted by red rectangles. Although of weaker magnitude [see areas marked in pink in Fig. 5(b)], a similar

observation has been made for the FGT/WSe₂ heterostructures for measurements up to 8 K.

The identification of spin textures via magnetotransport investigations is challenging and has been under intense debate [28]. Therefore, further investigations are required in order to understand in great detail the results reported here. This includes imaging the potential topological spin structures with methods, such as Lorentz TEM [21], for both pure FGT films and the heterostructures. This will allow for an unambiguous verification of the formation of spin textures, as well as to verify whether they are intrinsic to the FGT layer [21], or associated proximity-induced phenomena taking place at the vdW heterointerfaces [26].

IV. CONCLUSION

We have realized large-area epitaxial 2-D heterostructures of FGT/graphene and FGT/WSe₂ with good structural quality and high temperature ferromagnetic order. Results comparable or even superior to what has been reported for the state-of-the-art FGT flakes and related heterostructures could be demonstrated, however, on a large-scale. Hence, these results are highly relevant for the future realization of ultracompact 2-D spintronic devices based on 2-D magnetic materials and related heterostructures.

ACKNOWLEDGMENT

The authors would like to thank H.-P. Schönherr, C. Hermann, C. Stemmler, and K. Morgenroth for their technical support. They also appreciate the critical reading of the manuscript by Van Dong Pham.

This work was supported by the Penn State 2D Crystal Consortium-Materials Innovation Platform (2DCC-MIP) under NSF cooperative under Agreement DMR-2039351.

REFERENCES

- Y.-C. Lin et al., "Recent advances in 2D material theory, synthesis, properties, and applications," ACS Nano, vol. 17, no. 11, pp. 9694–9747, Jun. 2023, doi: 10.1021/acsnano.2c12759.
- [2] J. F. Sierra, J. Fabian, R. K. Kawakami, S. Roche, and S. O. Valenzuela, "van der Waals heterostructures for spintronics and opto-spintronics," *Nat. Nanotechnol.*, vol. 16, no. 8, pp. 856–868, 2021, doi: 10.1038/s41565-021-00936-x.
- [3] H. Yang et al., "Two-dimensional materials prospects for non-volatile spintronic memories," *Nature*, vol. 606, no. 7915, pp. 663–673, Jun. 2022, doi: 10.1038/s41586-022-04768-0.
- [4] B. Zhao et al., "A room-temperature spin-valve with van der Waals ferromagnet Fe₅GeTe₂/graphene heterostructure," Adv. Mater., vol. 35, no. 16, Apr. 2023, Art. no. 2209113, doi: 10.1002/adma.202209113.
- [5] J. M. J. Lopes et al., "Large-area van der Waals epitaxy and magnetic characterization of Fe₃GeTe₂ films on graphene," 2D Mater., vol. 8, no. 4, Aug. 2021, Art. no. 041001, doi: 10.1088/2053-1583/ac171d.
- [6] M. Ribeiro et al., "Large-scale epitaxy of two-dimensional van der Waals room-temperature ferromagnet Fe₅GeTe₂," NPJ 2D Mater. Appl., vol. 6, no. 1, p. 10, Feb. 2022, doi: 10.1038/s41699-022-00285-w.
- [7] Q. Guillet et al., "Epitaxial van der Waals heterostructures of Cr₂Te₃ on two-dimensional materials," *Phys. Rev. Mater.*, vol. 7, no. 5, May 2023, Art. no. 054005, doi: 10.1103/physrevmaterials.7.054005.
- [8] E. Georgopoulou-Kotsaki et al., "Significant enhancement of ferromagnetism above room temperature in epitaxial 2D van der Waals ferromagnet Fe₅-δGeTe₂/Bi₂Te₃ heterostructures," *Nanoscale*, vol. 15, no. 5, pp. 2223–2233, Feb. 2023, doi: 10.1039/d2nr04820e.

- [9] H. Kurebayashi, J. H. Garcia, S. Khan, J. Sinova, and S. Roche, "Magnetism, symmetry and spin transport in van der Waals layered systems," *Nature Rev. Phys.*, vol. 4, no. 3, pp. 150–166, Jan. 2022, doi: 10.1038/s42254-021-00403-5.
- [10] A. F. May et al., "Ferromagnetism near room temperature in the cleavable van der Waals crystal Fe₅GeTe₂," ACS Nano, vol. 13, no. 4, pp. 4436–4442, Apr. 2019, doi: 10.1021/acsnano.8b09660.
- [11] J. Seo et al., "Nearly room temperature ferromagnetism in a magnetic metal-rich van der Waals metal," Sci. Adv., vol. 6, no. 3, Jan. 2020, Art. no. eaay8912, doi: 10.1126/sciadv.aay8912.
- [12] H. Lv et al., "Large-Area synthesis of ferromagnetic $Fe_{5-x}GeTe_2/graphene$ van der Waals heterostructures with Curie temperature above room temperature," *Small*, vol. 19, no. 39, Sep. 2023, Art. no. 2302387, doi: 10.1002/smll.202302387.
- [13] M. Heilmann, A. S. Prikhodko, M. Hanke, A. Sabelfeld, N. I. Borgardt, and J. M. J. Lopes, "Influence of proximity to supporting substrate on van der Waals epitaxy of atomically thin graphene/hexagonal boron nitride heterostructures," ACS Appl. Mater. Inter., vol. 12, no. 7, pp. 8897–8907, Feb. 2020, doi: 10.1021/acsami.9b21490.
- [14] H. Zhu et al., "Step engineering for nucleation and domain orientation control in WSe₂ epitaxy on *c*-plane sapphire," *Nature Nanotechnol.*, vol. 18, no. 11, pp. 1295–1302, Nov. 2023, doi: 10.1038/s41565-023-01456-6
- [15] L. Kang et al., "Phase-controllable growth of ultrathin 2D magnetic FeTe crystals," *Nature Commun.*, vol. 11, no. 1, p. 3729, Jul. 2020, doi: 10.1038/s41467-020-17253-x.
- [16] B. Dieny and M. Chshiev, "Perpendicular magnetic anisotropy at transition metal/oxide interfaces and applications," Rev. Mod. Phys., vol. 89, no. 2, Jun. 2017, Art. no. 025008, doi: 10.1103/RevMod-Phys.89.025008.
- [17] Y. Huang, X. Yao, F. Qi, W. Shen, and G. Cao, "Anomalous resistivity upturn in the van der Waals ferromagnet Fe₅GeTe₂," *Appl. Phys. Lett.*, vol. 121, no. 16, Oct. 2022, Art. no. 162403, doi: 10.1063/5.0109735.
- [18] H. Zhang et al., "Itinerant ferromagnetism in van der Waals Fe_{5-x}GeTe₂ crystals above room temperature," *Phys. Rev. B, Condens. Matter*, vol. 102, no. 6, Aug. 2020, Art. no. 064417, doi: 10.1103/phys-revb.102.064417.
- [19] W. Miao et al., "Nonreciprocal antisymmetric magnetoresistance and unconventional Hall effect in a two-dimensional ferromagnet," ACS Nano, vol. 17, no. 24, pp. 25449–25458, Dec. 2023, doi: 10.1021/acsnano.3c08954.
- [20] A. F. May, C. A. Bridges, and M. A. McGuire, "Physical properties and thermal stability of Fe_{5-x}GeTe₂ single crystals," *Phys. Rev. Mater.*, vol. 3, no. 10, Oct. 2019, Art. no. 104401, doi: 10.1103/PhysRevMaterials.3.104401.
- [21] M. Schmitt et al., "Skyrmionic spin structures in layered Fe₅GeTe₂ up to room temperature," *Commun. Phys.*, vol. 5, no. 1, p. 254, Oct. 2022, doi: 10.1038/s42005-022-01031-w.
- [22] Y. Gao et al., "Spontaneous (anti)meron chains in the domain walls of van der Waals ferromagnetic Fe_{5-x}GeTe₂," Adv. Mater., vol. 32, no. 48, Dec. 2020, Art. no. 2005228, doi: 10.1002/adma.202005228.
- [23] Y. Deng et al., "Layer-number-dependent magnetism and anomalous Hall effect in van der Waals ferromagnet Fe₅GeTe₂," *Nano Lett.*, vol. 22, no. 24, pp. 9839–9846, Dec. 2022, doi: 10.1021/acs.nanolett.2c02696.
- [24] M.-H. Phan et al., "Exchange bias and interface-related effects in two-dimensional van der Waals magnetic heterostructures: Open questions and perspectives," *J. Alloys Compounds*, vol. 937, Mar. 2023, Art. no. 168375, doi: 10.1016/j.jallcom.2022.168375.
- [25] L. Zhang et al., "Proximity-coupling-sinduced significant enhancement of coercive field and Curie temperature in 2D van der Waals heterostructures," Adv. Mater., vol. 32, no. 38, Sep. 2020, Art. no. 2002032, doi: 10.1002/adma.202002032.
- [26] Y. Wu et al., "Néel-type skyrmion in WTe₂/Fe₃GeTe₂ van der Waals heterostructure," *Nature Commun.*, vol. 11, no. 1, p. 3860, Jul. 2020, doi: 10.1038/s41467-020-17566-x.
- [27] P. K. Sivakumar et al., "Topological Hall signatures of two chiral spin textures hosted in a single tetragonal inverse Heusler thin film," ACS Nano, vol. 14, no. 10, pp. 13463–13469, Oct. 2020, doi: 10.1021/acsnano.0c05413.
- [28] G. Kimbell, C. Kim, W. Wu, M. Cuoco, and J. W. A. Robinson, "Challenges in identifying chiral spin textures via the topological Hall effect," *Commun. Mater.*, vol. 3, no. 1, p. 19, Apr. 2022, doi: 10.1038/s43246-022-00238-2.